Influence of membrane lipid composition on the structure and activity of γ-secretase

Rodrigo Aguayo-Ortiz[a], John E. Straub[b], and Laura Dominguez[a,*]

[a]Facultad de Química, Departamento de Fisicoquímica, Universidad Nacional Autónoma de México, Mexico City, 04510, Mexico
[b]Department of Chemistry, Boston University, Boston, Massachusetts 02215, USA

***Corresponding Author:** Phone: +52-5622-3773. E-mail: lauradd@unam.mx

Table of contents

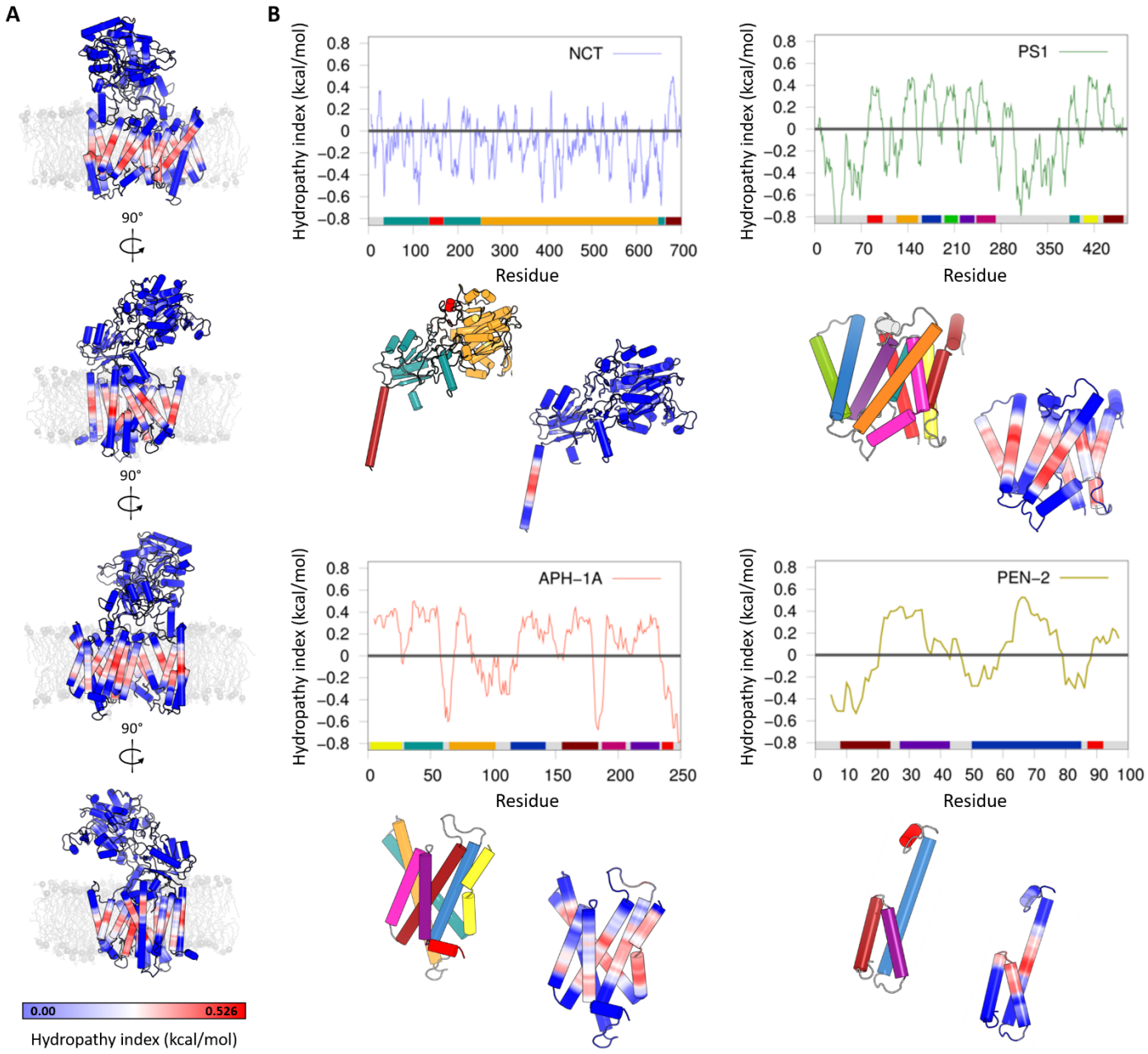

Figure S1. (A) Depiction of the hydropathy index distribution ranging from the most (blue) to the least hydrophilic (red) regions. (B) Hydropathy plots for the four γ-secretase (GS) components. The figures beneath the plots depict the 3D structure of the GS subunit color coded by the TMs and the hydropathy index.

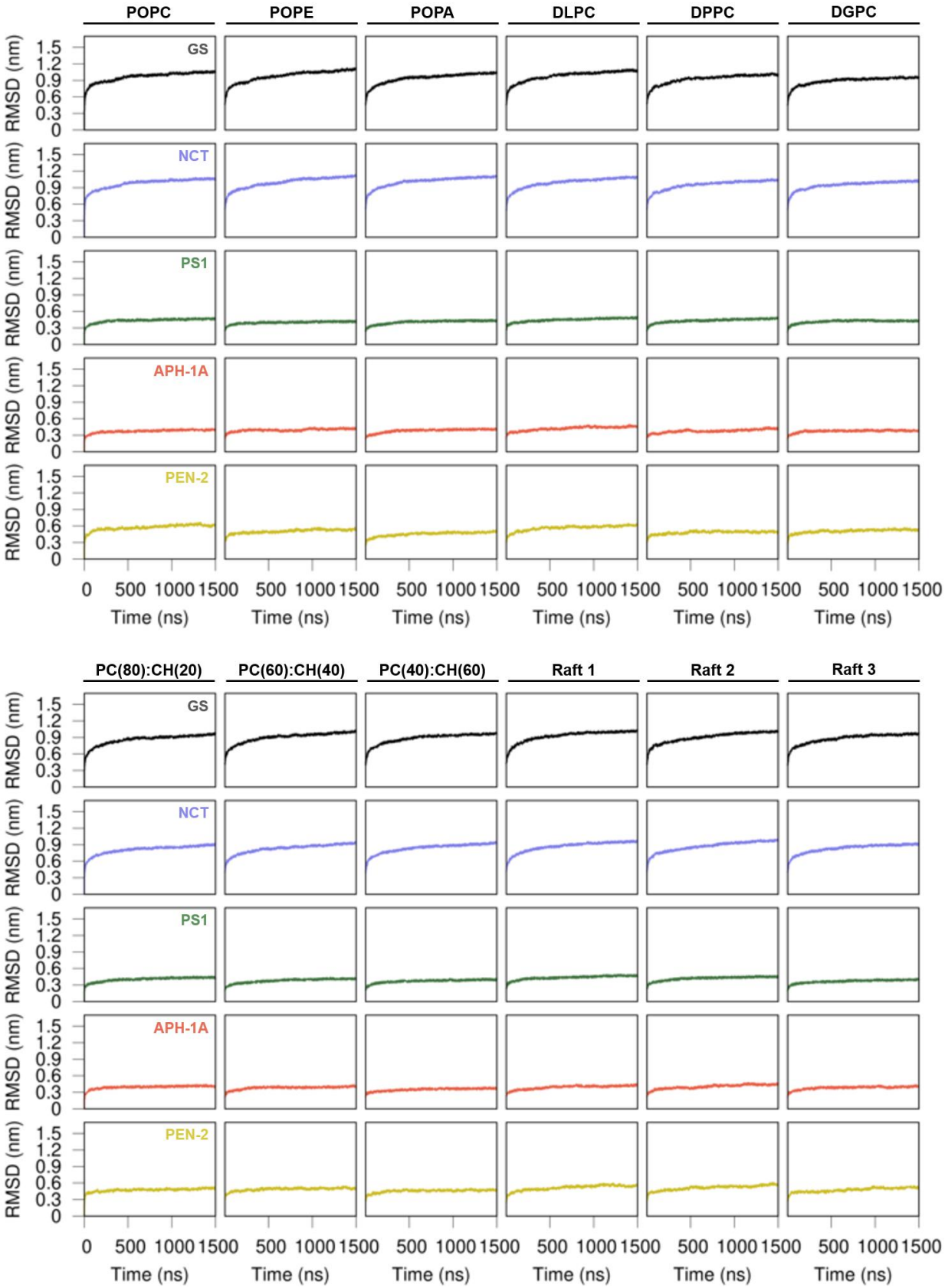

Figure S2. Root-mean-squared deviation (RMSD) average of the 20 replicas from the unprotonated Asp385 GS 5FN2 derived coarse-grained (CG) models in twelve different lipid membranes.

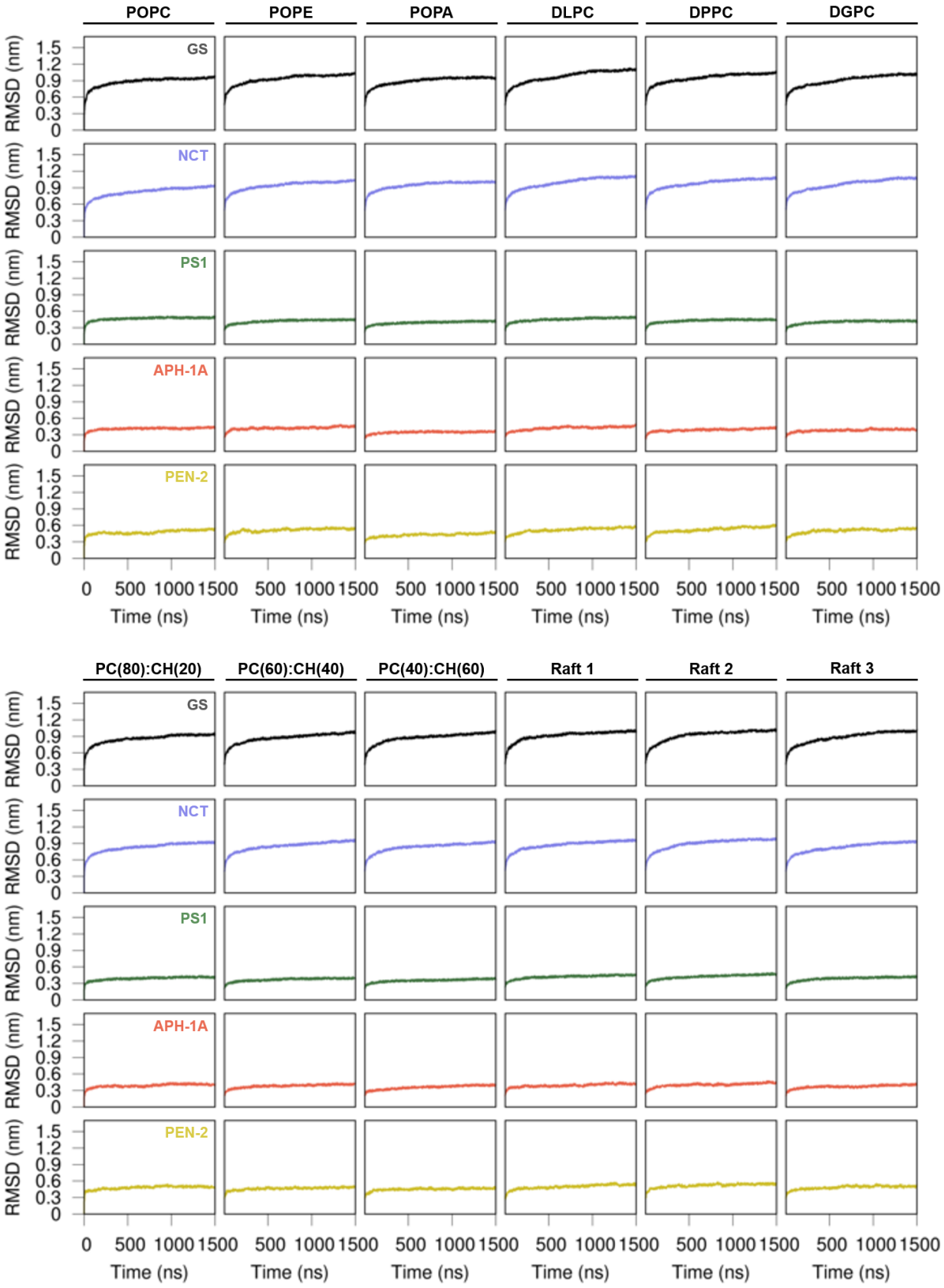

Figure S3. Root-mean-squared deviation (RMSD) average of the 20 replicas from the protonated Asp385 GS 5FN2 derived coarse-grained (CG) models in twelve different lipid membranes.

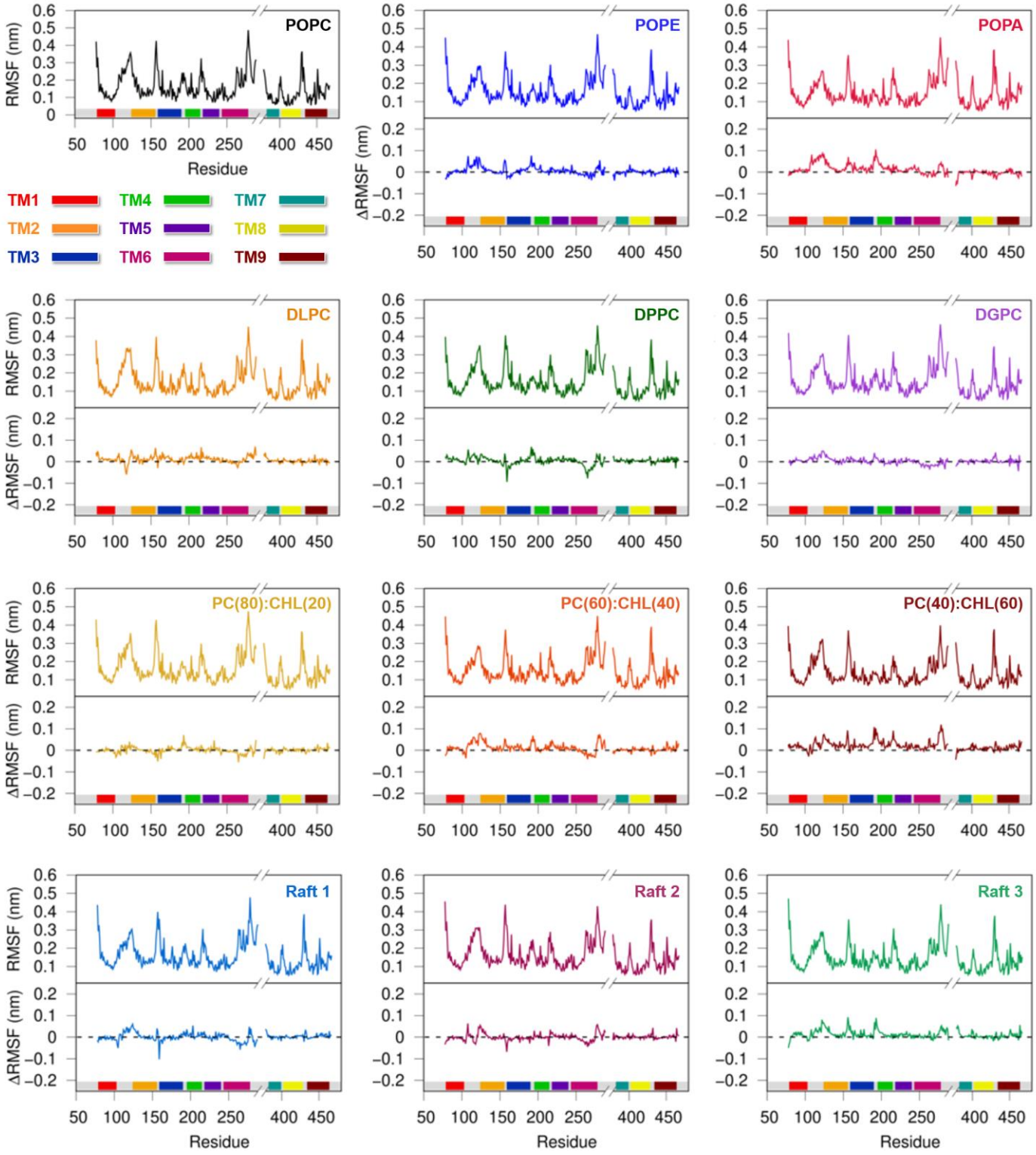

Figure S4. Root-mean-squared fluctuation (RMSF) average (*Top plot*) and RMSF difference (*Bottom plot*) between the GS-POPC and each GS-Lipid system of the last 500 ns of the 20 replicas from the unprotonated Asp385 GS5FN2 derived coarse-grained (CG) models. The colored bar at the bottom of the graphs indicates the location of each TM in the PS1 sequence.

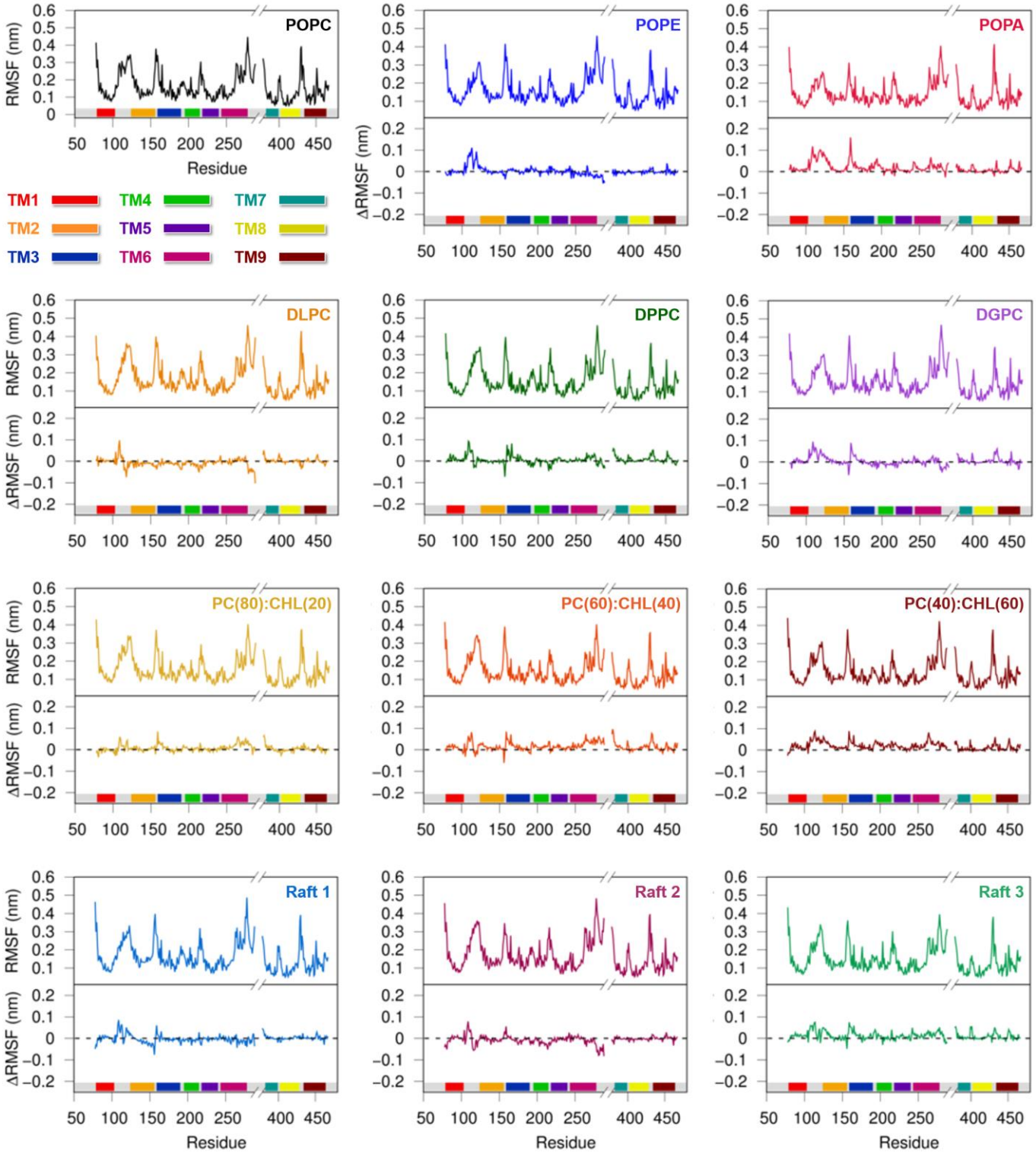

Figure S5. Root-mean-squared fluctuation (RMSF) average (*Top plot*) and RMSF difference (*Bottom plot*) between the GS-POPC and each GS-Lipid system of the last 500 ns of the 20 replicas from the protonated Asp385 GS5FN2 derived coarse-grained (CG) models. The colored bar at the bottom of the graphs indicates the location of each TM in the PS1 sequence.

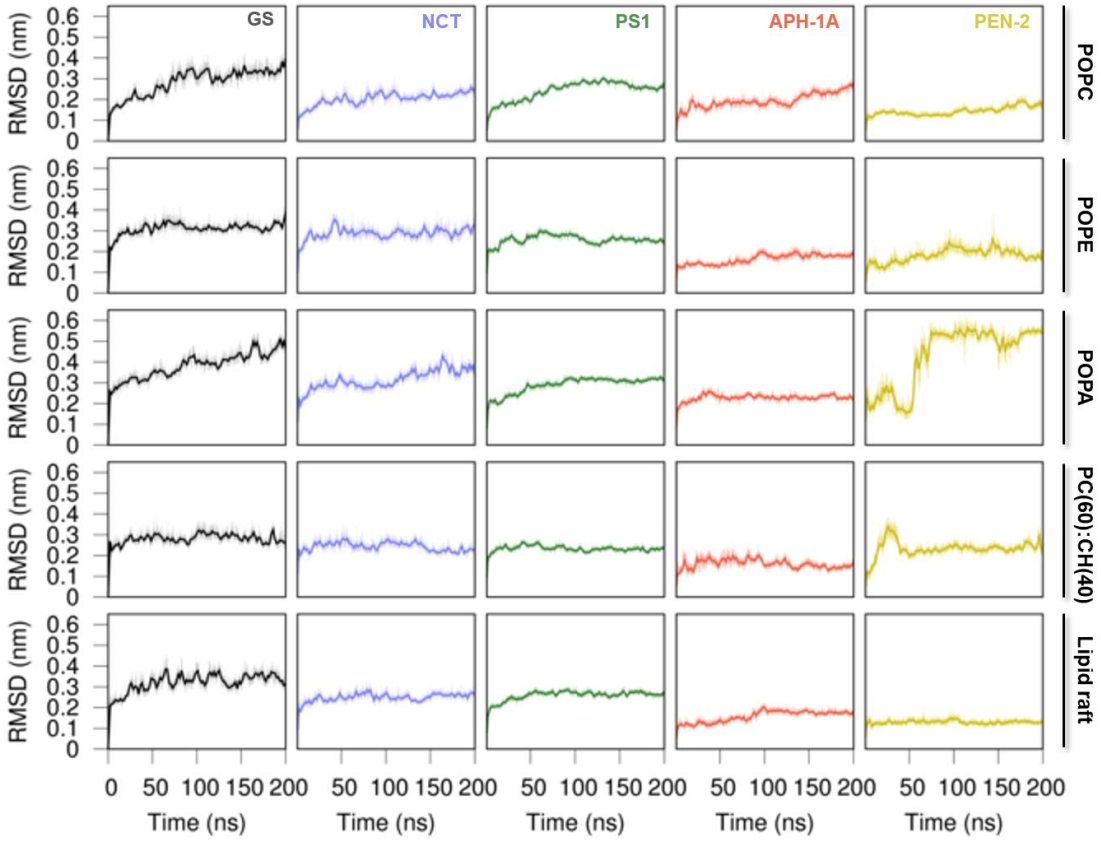

Figure S6. Root-mean-squared deviation (RMSD) of GS derived all-atom (AA) models in five different lipid membranes.

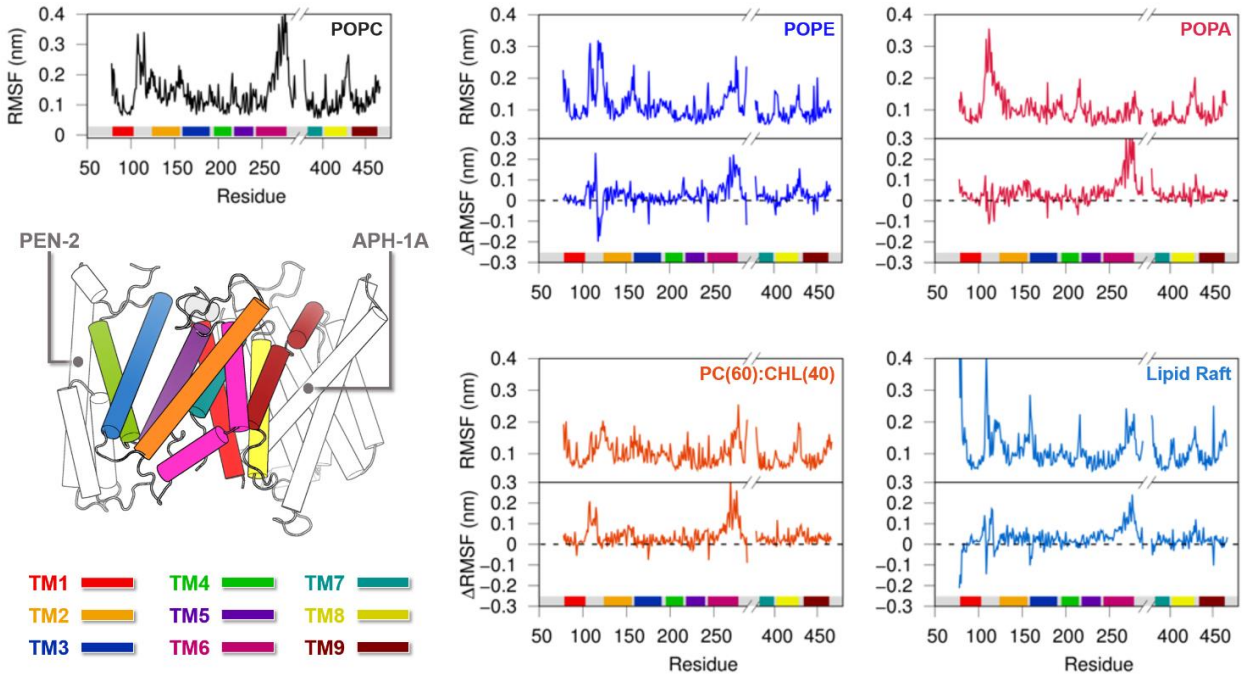

Figure S7. Root-mean-squared fluctuation (RMSF) (*Top plot*) and RMSF difference (*Bottom plot*) between the GS-POPC and each GS-Lipid system of the last 100 ns of GS derived all-atom (AA) models. The colored bar at the bottom of the graphs indicates the location of each TM in the PS1 sequence as the 3D structure located at the left-bottom corner of the figure.

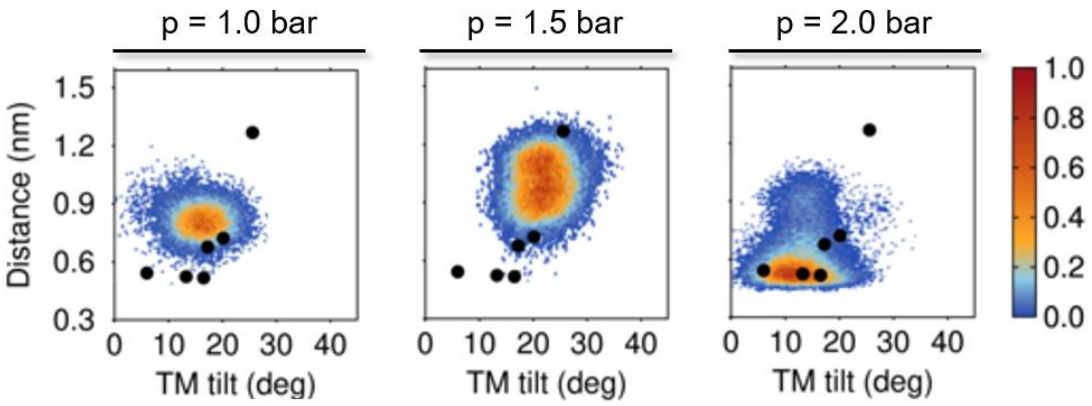

Figure S8. Distribution of GS-POPC CG simulations at three different pressures projected onto the distances between the catalytic residues (Asp257 and Asp385) and the calculated TM6 tilt angles.

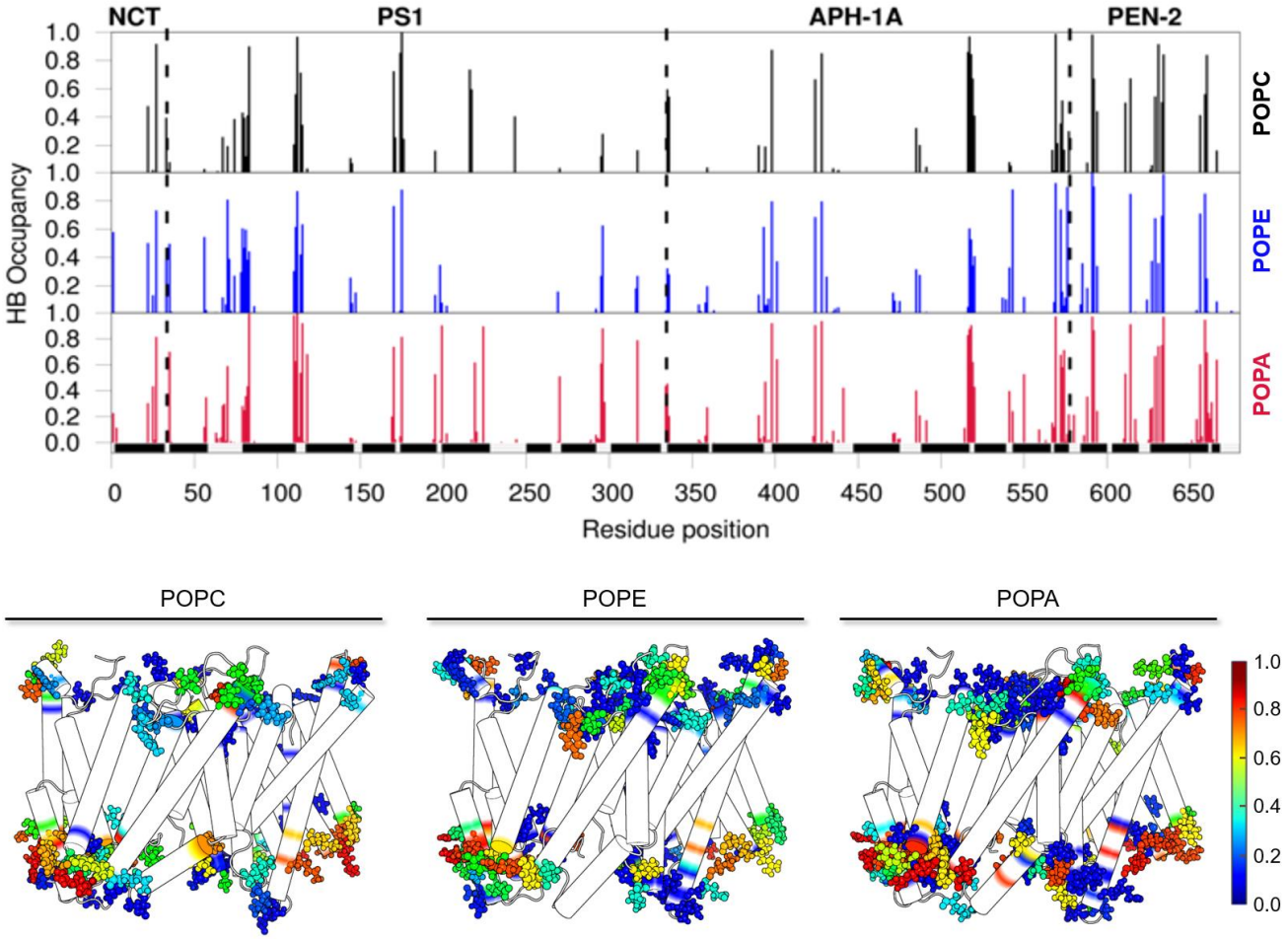

Figure S9. GS-lipid hydrogen bond occupancies through the last 100 ns of the atomistic MD simulations GS embedded in POPC (black), POPE (blue) and POPA (red). The 3D structures located beneath the plot depict the amino acids involved in the formation of hydrogen bonds with the lipids (color coded from the higher (red) to the lower (blue) occupancy values).

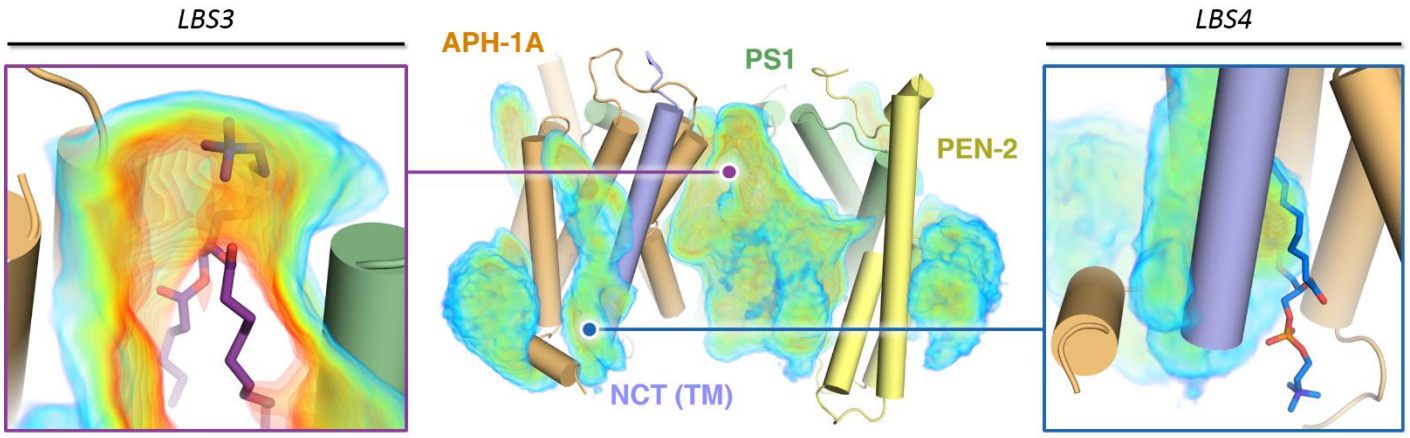

Figure S10. Superposition of experimentally solved distearoyl-phosphatidylcholine lipids in 5A63[1] structure onto the 3D density distribution of the selected POPC lipids from the GS derived all-atom (AA) models with high residence times. For this study, the positions of the lipids were assigned to the lipid binding sites (LBS) 3 and 4.

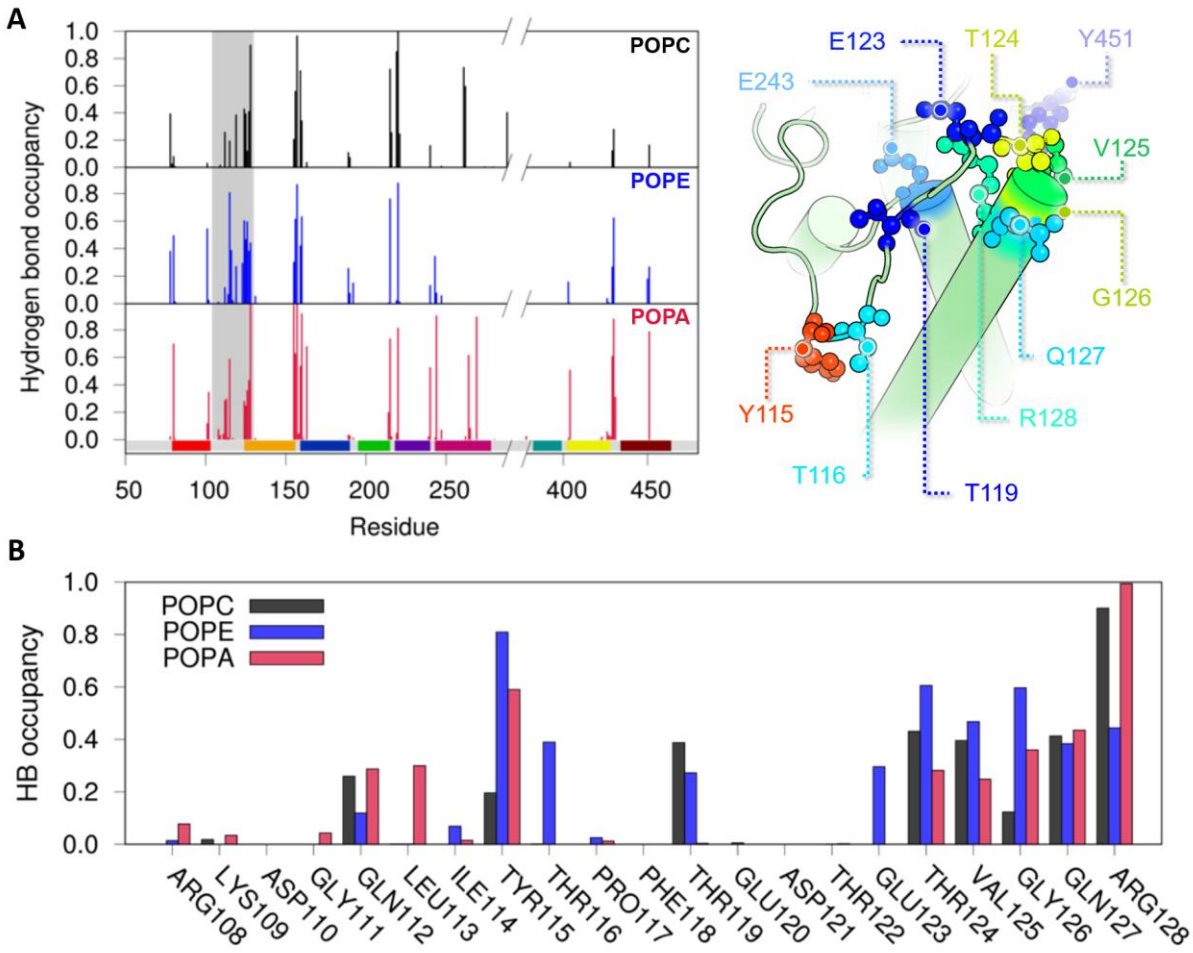

Figure S11. (A) GS-lipid hydrogen bond occupancies through the last 100 ns of the atomistic MD simulations. The gray shadow in the plot highlights the HL1 loop region. (B) GS-lipid hydrogen bond occupancies of the HL1 loop and TM2 N-terminal region. The 3D structure located at the right-top corner of the figure depicts the amino acids involved in the formation of hydrogen bonds with POPE (color coded from the higher (red) to the lower (blue) occupancy values).

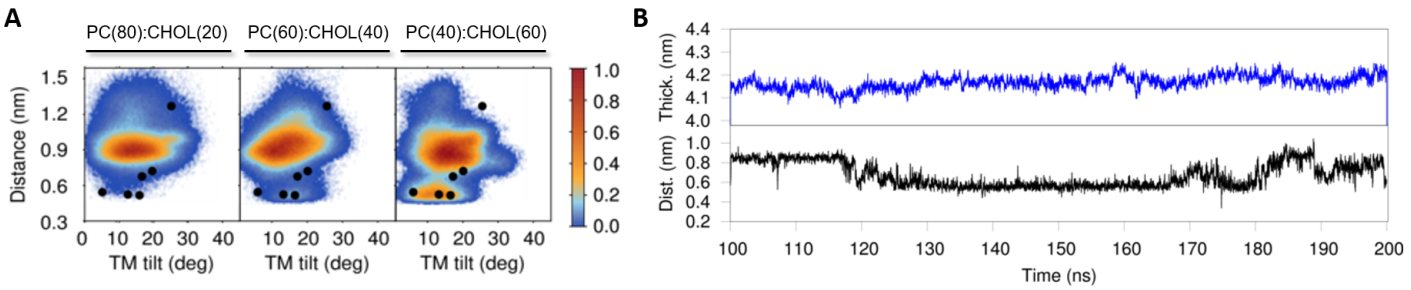

Figure S12. (A) Distribution of GS CG simulations in POPC:CHOL lipid bilayers projected onto the distances between the catalytic residues (Asp257 and Asp385) and the calculated TM6 tilt angles in the unprotonated state of Asp385. The colored scale on the *Right* defines the relative populations. The black circles depict the values obtained from experimental structures of GS at CG resolution after backbone-restrained minimization (PDB IDs: 5A63, 4UIS, 5FN2, 5FN3, 5FN4 and 5FN5).[1–3] (B) Time evolution of POPC(60):CHOL(40) membrane thickness (*Top*) and the minimum distance between the catalytic aspartics and cholesterol (*Bottom*) through the last 100 ns of the atomistic MD simulations.

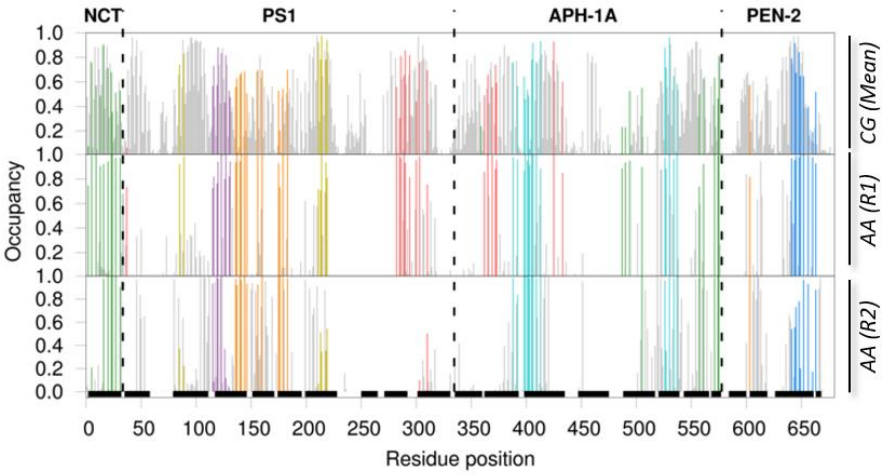

Figure S13. Per amino acid occupancy of GS and CHOL contacts during the CG (average of the 20 replicas) and all-atom (R1: replica 1, and R2: replica 2) simulations.

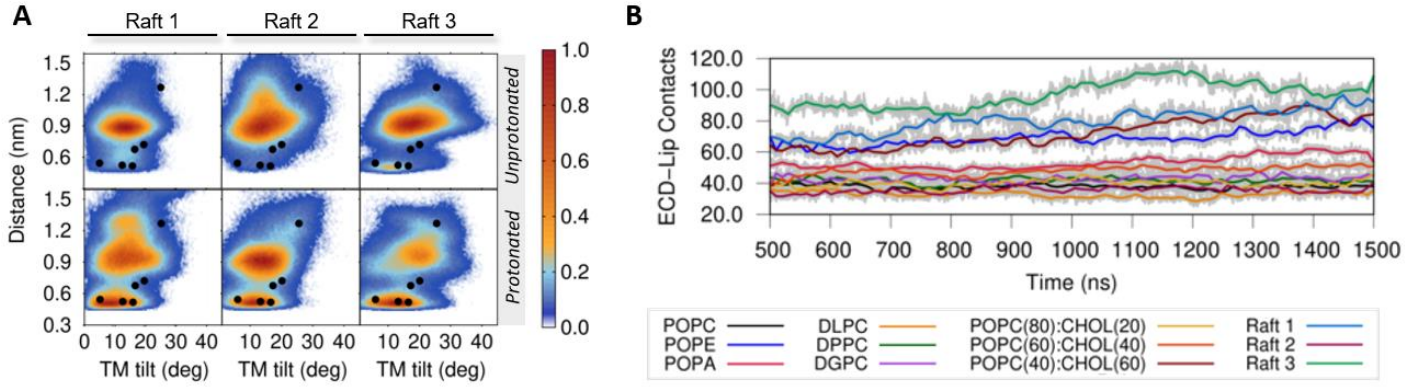

Figure S14. (A) Distribution of GS CG simulations in the three lipid rafts projected onto the distances between the catalytic residues (Asp257 and Asp385) and the calculated TM6 tilt angles in the unprotonated state of Asp385. The colored scale on the *Right* defines the relative populations. The black circles depict the values obtained from experimental structures of GS at CG resolution after backbone-restrained minimization (PDB IDs: 5A63, 4UIS, 5FN2, 5FN3, 5FN4 and 5FN5).[1–3] (B) Average of the number of contacts between the NCT ECD and the lipid headgroups (Lip) in the ten CG models.

Table S1. Amino acids that constitutes the lipid and cholesterol binding sites.

Binding Site	Subunit	Amino acids
SBS1	PS1	I416, C419, L420, L423, L424, I427, F428, K430, P433, I437, F441, V444
	APH-1A	L30, I33, A37, F40, F41, V44, L81, L82, V85, F86, F88, A89, K92, L93, K96, A97, L101, Y187, L190, V194, L198
SBS2	PS1	W203, V207, I211, W215
	PEN-2	R16, K17, Y19, L20, G21, F23, F25, W30, Y56, W58, R59, V62, L65, F66, W67, I69, V70
LBS1	PS1	Q112, I114, Y115, V142, M146, L149, W165, I168, S169, L172, L173, F176, F177, M233, V236, F237, Y240
LBS2	PS1	V125, R128, A129, L130, I133, L134, I140, I143, E243, W244, L248, I249, V252, T256
LBS3	PS1	V87, T90, L91, V94, V95, A98, K101, S102, Y181, L182, Y189, L201, F205, R220, L221, A224, I227, M228, W404, T407, I408, F411
	PEN-2	F28, L31
LBS4	NCT	E667, L670, I671, T674, V675, F677, G678, I679, F682, I685, V686, C689, I690, K693, L697
	APH-1A	P16, L20, Y119, L158, T159, F162, L169, F173, L215, Y218, V222, L226, F229, L236, R237, I239, Q240, S242, L243, L244
CBS1	PS1	K160, V161, A164, W165, I168, L171, L172, F175, F176
CBS2	PS1	V125, A129, L130, I133, L134, A136, I140, V144, W244, L248, I249, A251, V252, V255, T256, L258, V259, C263, P264
CBS3	PS1	V82, I416, C419, L420, L423, L424, F428, A434, I437, V444
	APH-1A	L30, I33, A37, F40, F41, L93, L101
CBS4	APH-1A	L56, T60, R66, L67, Y69, G70, L71, I73, F74, A77, L81, V194, G195, L198, G202, F205
CBS5	NCT	I671, V675, I679, F682, V686, C689, I690, K693, L697
	APH-1A	G27, Y155, L158, F162, F173, G225, F229, I239, S242, L243
CBS6	PS1	Y181, L182, V185, F186, Y189, V191, L201, F205, R220, L221, A224, M228
	PEN-2	F28
CBS7	PEN-2	F66, I69, V70, S73, W74, I77, Y81, W85, L88

References

1 X. Bai, C. Yan, G. Yang, P. Lu, D. Ma, L. Sun, R. Zhou, S. H. W. Scheres and Y. Shi, *Nature*, 2015, **525**, 212–7.

2 L. Sun, L. Zhao, G. Yang, C. Yan, R. Zhou, X. Zhou, T. Xie and Y. Zhao, *Proc. Natl. Acad. Sci. U. S. A.*, 2015, **112**, 6003–6008.

3 X.-C. Bai, E. Rajendra, G. Yang, Y. Shi and S. H. Scheres, *Elife*, 2015, **4**, e11182.